1972MNRAS.158..383D

Mon. Not. R. astr. Soc. (1972) **158**, 383–403.

THE STRUCTURE AND EVOLUTION OF HELIUM STARS

Ann St Clair Dinger

(Received 1972 March 6)

SUMMARY

Numerical models of helium stars have been constructed in an effort to fit the models to the observed extreme-helium stars, i.e. those which have equivalent spectral types of O7-B5, absolute magnitudes brighter than $-1{\cdot}6$, and weak or missing hydrogen lines.

Main-sequence models of 1, 2, 4 and 8 $M_\odot$ were computed for $Y = 0{\cdot}98$, $Z = 0{\cdot}02$. The effect of the inclusion of the $N^{14}(\alpha, \gamma)F^{18}(e^+\nu)O^{18}$ reaction was investigated. It is shown that the addition of 10^{-3} of hydrogen by mass had a negligible effect on these models. One-solar-mass models with 2, 6, 14, 30 and 58 per cent additional carbon were also computed. Carbon enrichment increased the luminosity, effective temperature and central temperature of the model and decreased the central density. A four-solar-mass model with $Z = 0{\cdot}60$ ($0{\cdot}02$ solar metals and $0{\cdot}58$ additional carbon) was also computed.

The four-solar-mass $Z = 0{\cdot}02$ and $Z = 0{\cdot}60$ models were evolved until carbon ignited in their cores under non-degenerate conditions. The evolution of the one-solar-mass, $Z = 0{\cdot}60$ model was followed to the white dwarf state. Computations of the evolution of the one-solar-mass, $Z = 0{\cdot}02$ model were stopped when the mass of the helium-exhausted core was $0{\cdot}767\ M_\odot$. This model crossed the main sequence for hydrogen-burning in the region of the observed helium stars and evolved toward the red giant region of the H–R diagram.

I. INTRODUCTION

The known helium-rich stars can be divided into five distinct classes (Hack 1967; Dinger 1970, 1971), the O-subdwarfs, the extreme-helium stars, the moderate-helium stars, the close binaries similar to β Lyr and the R CrB stars. It is believed that some of the carbon stars may also be helium rich. The important properties of the helium-rich stars are summarized in Table I. They differ in position on the H–R diagram, population type, estimated mass, helium-to-hydrogen ratio and the abundances of carbon, nitrogen, and oxygen. These three elements are especially important, as their relative abundances change during hydrogen and helium burning and provide clues to the nuclear processes that have produced the observed abundances.

The close binaries are the only helium-rich stars for which there is any evidence of a close companion and possible mass exchange which could be used to explain the observed abundances. However, their varying abundances and luminosity classes clearly separate the close binaries from the rest of the helium-rich stars, which form quite homogeneous groups. Extensive mass loss and mixing of nuclear reaction products to the surface at different evolutionary phases could explain the existence of the other four types of helium-rich stars. The O-subdwarfs show evidence of the products of the CNO cycle, while the R CrB and extreme helium stars exhibit the high carbon and lower nitrogen and oxygen

Downloaded from https://academic.oup.com/mnras/article/158/4/383/2603087 by guest on 26 January 2026

© Royal Astronomical Society • Provided by the NASA Astrophysics Data System

1972MNRAS.158..383D

TABLE I

Types of helium-rich stars

Type	Spectrum	M_V (est.)	Population	Mass (est.) $M_\odot$	He/H[a]	Other abundances C	N	O
O-subdwarfs	Early O	+3 to +4	Int. Pop. I	0·5?	0·15–2·5	–	+	–
Extreme He	O7–B5	≤ −1	Int. Pop. II	>0·5	>10[3]	+	+	–
Moderate He	B1–B8	≤ 0	Pop. I	~10	1–2	Near normal		
Close Binaries	B8–A3	−1·5 to −5·5	Pop. I?	?	2–10[4]	Varies		
R CrB Variables	B2–R8	−5	Pop. I?	~1?	2–3	+	?	?

[a] Ratio by number.

Downloaded from https://academic.oup.com/mnras/article/158/4/383/2603087 by guest on 26 January 2026

© Royal Astronomical Society • Provided by the NASA Astrophysics Data System

1972MNRAS.158..383D

abundances that characterize the early stages of helium burning. It would seem that a large proportion of the original hydrogen-rich envelope has been retained in the moderate-helium stars.

Several authors have calculated evolutionary models of helium stars, either pure helium or helium and heavy elements, and these are immediately relevant to the stars observed to have negligible amounts of hydrogen, i.e. the O-subdwarfs and the extreme helium stars. Homogeneous, pure helium 'main sequence' models have been computed by Crawford (1953), Cox & Giuli (1961), Hayashi, Hoshi & Sugimoto (1962), Osaki (1963), Van der Borght & Meggitt (1963), Cox & Salpeter (1964), Deinzer & Salpeter (1964), and L'Ecuyer (1966). $Y = 0{\cdot}999$ and $Z = 0{\cdot}001$ were used for Oke's (1961) one-solar-mass model and Divine's (1965) main sequence, while Aller (1959) used $Y = 0{\cdot}99$, $Z = 0{\cdot}01$. These main sequence models are qualitatively similar. The exact numerical results depend on the nuclear

TABLE II

Helium-star models computed by various authors

$M/M_\odot$	Author	$R/R_\odot$	$\log L/L_\odot$	$\log T_e$	$\log T_c$	$\log \rho_c$	M_{cc}/M
1·0	Oke	0·175	2·4871	4·7604	8·1682	3·482	0·2619
	Cox & Giuli	0·1689	2·5057	4·7747	8·1430	3·7622	—
	Cox & Salpeter	0·168	2·467	4·766	8·1278	3·7470	0·3121
	Divine	0·1866	2·3617	4·7182	8·1219	3·7781	0·2640
	L'Ecuyer	0·182	2·4572	4·746	8·130	3·769	0·257
	Dinger	0·1994	2·3723	4·7055	8·1189	3·7727	0·2684
2·0	Cox & Giuli	0·2985	3·4088	3·8769	8·1967	3·3214	—
	Cox & Salpeter	0·3047	3·397	4·869	8·1824	3·2883	0·3120
	Divine	0·3166	3·3541	4·8513	8·1732	3·3727	0·3216
	Dinger	0·3326	3·3585	4·8410	8·1697	3·3705	0·3335
4·0	Cox & Giuli	0·5198	4·3119	4·9822	8·2570	2·8999	—
	Cox & Salpeter	—	—	4·96	8·2423	2·8587	0·3120
	Divine	0·5023	4·2095	4·9649	8·2187	3·0444	0·4307
	Dinger	0·5221	4·2018	4·9539	8·2140	3·0483	0·4509
8·0	Cox & Giuli	0·8884	5·2150	5·0917	8·3251	2·5027	—
	Cox & Salpeter	—	—	5·08	8·3090	2·4548	0·3120
	Divine	0·7635	4·9279	5·0538	8·2562	2·8044	0·5962
	Dinger	0·7777	4·8986	5·0415	8·2507	2·7915	0·5968

reactions considered, the reaction rates adopted, the treatment of the opacity, and the inclusion or exclusion of the effects of radiation pressure and electron degeneracy. On the H–R diagram these main sequences are roughly parallel to, but well to the left of, the normal hydrogen-burning main sequence. The low mass ends ($0{\cdot}3$–$0{\cdot}5\ M_\odot$) cut through the region occupied by the O-subdwarfs and the nuclei of planetary nebulae. Table II compares the results of these various computations to those of the present work, in which a higher abundance of heavy elements was assumed.

Evolutionary tracks from the helium main sequence have been computed by Aller (1959), Hayashi *et al.* (1962), Osaki (1963), Cox & Salpeter (1964), Deinzer & Salpeter (1964), and Divine (1965). Helium-burning stars with hydrogen-rich envelopes were considred by Cox & Salpeter (1961) and Osaki (1963), while Rose (1966) studied the shell-burning phases of stars with pure helium envelopes. All of the tracks are characterized by an initial rise in luminosity, a hook to higher effective temperatures at nearly constant luminosity, an abrupt change to a rapid

Downloaded from https://academic.oup.com/mnras/article/158/4/383/2603087 by guest on 26 January 2026

© Royal Astronomical Society • Provided by the NASA Astrophysics Data System

1972MNRAS.158..383D

rise in luminosity at nearly constant effective temperature followed by a gradual change to a rapid decrease in effective temperature with slowly increasing luminosity. Cox & Salpeter and also Deinzer & Salpeter followed their models to the phase of core helium exhaustion, while Aller, Hayashi *et al.*, Osaki and Divine continued until the helium-burning shell was well established.

The present work extends the study of helium-star models to more realistic abundances and more extended evolutionary tracks. Attempts to fit the models to the observed extreme-helium stars determine the masses and compositions used. The solar basic metal abundance of $Z = 0{\cdot}02$ was adopted since near-solar abundances of the heavy elements have been deduced for the extreme-helium stars (Hill 1965). The abundance ranges of $0–10^{-3}$ for hydrogen and $0{\cdot}003–0{\cdot}58$ for carbon bracket the abundances quoted in the literature. One solar mass was the lowest mass considered, since this investigation deals with models that were expected to evolve to the right on the H–R diagram after core helium burning, rather than immediately becoming white dwarfs. Four-solar-mass models were also evolved, as they were expected to pass through the upper part of the region of the H–R diagram occupied by the extreme-helium stars. The properties of the extreme-helium stars are discussed by Dinger (1970).

An initial abundance of $Y = 0{\cdot}98$, $Z = 0{\cdot}02$, with heavy elements in the solar proportion, is used. It is shown that the addition of 0·1 per cent of hydrogen by mass to the outer envelope has a negligible effect on the stellar model. Radiative opacities on the model of Cox & Stewart (computed at the author's request for 10 carbon-rich mixtures) allow the computation of models with additional carbon. In these mixtures carbon is added to the basic abundances of $Y = 0{\cdot}98$, $Z = 0{\cdot}02$, and $X = 0{\cdot}20$, $Y = 0{\cdot}78$, $Z = 0{\cdot}02$ at the expense of helium. With the opacities for these mixtures it is possible to compute carbon-enriched models up to $Z = 0{\cdot}62$ (0·02 solar heavy elements and 0·60 extra carbon) for hydrogen abundances between 0 and 0·20. Models with these extremely large carbon abundances are used to examine Hunger & Klinglesmith's (1969) derivation of $X = 0{\cdot}001$, $Y = 0{\cdot}45$, $Z = 0{\cdot}55$ for BD+10°2179.

2. THE PROGRAM

The Henyey type program used for these computations was originally written by B. Paczynski. The program has been extensively discussed in the literature (Paczynski 1969, 1970a, b, c).

The core and the envelope of the models are integrated separately, with the results of the envelope integrations used as outer boundary conditions for the interior. For each mass and chemical composition, the table of boundary conditions gives the temperature, density, and radius at the bottom of the envelope and the effective temperature and radius of the star as functions of the surface temperature and luminosity. The nuclear reaction rates, the opacity coefficients, the neutrino emission rates and all the thermodynamic functions (pressure, the specific heats at constant pressure and density, and the adiabatic and radiative temperature gradients) are also computed in auxiliary programs and stored in the computer memory as functions of temperature and density.

The mathematical techniques of this envelope program are discussed by Paczynski (1969). It can be used for all phases of evolution, including the very extended envelopes of supergiants, since the dilution of radiation and non-adiabatic

Downloaded from https://academic.oup.com/mnras/article/158/4/383/2603087 by guest on 26 January 2026

© Royal Astronomical Society • Provided by the NASA Astrophysics Data System

1972MNRAS.158..383D

convection are taken into account. The mixing length is taken to be one pressure scale-height. The hydrogen and helium ionization zones and the dissociation of H_2 are considered in the computation of the pressure and of the internal energy per gramme. Since the interior is assumed to be completely ionized, the mass contained in the envelope must be large enough so that the temperature at the bottom of the envelope is at least 10^5°K.

Paczynski interpolated the radiative opacities, including lines, from the Cox & Stewart (1969) tables. Conductive opacities (Hubbard & Lampe 1969; Canuto 1969) and the opacity due to water vapour (Auman 1967) were also included.

Cox & Stewart computed the opacities of 10 carbon-rich mixtures at the author's request. These mixtures have $X = 0$ and $X = 0{\cdot}20$, each for $Z = 0{\cdot}04018$, $0{\cdot}07718$, $0{\cdot}15718$, $0{\cdot}31718$, and $0{\cdot}61718$, where $Z = 0{\cdot}01718 + Z_C$. The values of Z_C, the carbon abundance, are $0{\cdot}023$, $0{\cdot}06$, $0{\cdot}14$, $0{\cdot}30$ and $0{\cdot}60$, while the solar abundance of all elements heavier than carbon is assumed to be $0{\cdot}01718$. In the present investigation the opacity tables for $X = 0$ and $0{\cdot}20$ for $Z = 0{\cdot}004$ and $0{\cdot}02$ were used for the models not enriched by carbon. The table for $X = 0$, $C = O = 0{\cdot}478$ was used for the helium-exhausted core.

The energy generation rates were those of Reeves (1965) for hydrogen-burning, Fowler, Caughlan & Zimmerman (1967) for helium-burning, Patterson, Winkler & Zaidins (1969) for carbon-burning, and Reeves for oxygen-burning. The reactions considered were the p–p and CNO cycles, N+He, triple alpha, C+He, $C^{12}+C^{12}$, and $O^{16}+O^{16}$. Weak and strong screening corrections were used for all but hydrogen-burning reactions.

Neutrino emission rates for photo neutrinos, plasma neutrinos, and the neutrinos resulting from pair production were calculated from Beaudet, Petrosian & Salpeter (1967) and taken into account in all hydrogen-exhausted regions. Radiation pressure and the effects of relativistic velocities of the electrons, with or without electron degeneracy, were considered, but no particle interactions such as crystallization or pair production were included.

Paczynski (1970b) discussed the difficulties involved in determining the boundary of the expanding convective core during core helium burning. A sharp composition discontinuity soon develops at the edge of the core. The boundary of the convective core is determined by the ratio of the radiative and adiabatic temperature gradients, which, through the composition, depends on the amount of expansion that was assumed in the estimation of the model. This interdependence makes determination of the exact boundary uncertain.

The correct physical solution probably requires a semi-convective region between the convective core and the helium-rich envelope. Paczynski treated this computational problem by not allowing the convective core to move by more than 0·001 times the total mass of the star between consecutive models. Since the instability does not develop until several models have been computed, his method effectively keeps the computed boundary of the convective core at or near the boundary of the fully convective region. The core generally expands by the maxi mum amount until the phase of helium exhaustion, when the convective region starts shrinking rapidly. This method probably underestimates the mass of the convective region and the amount of helium mixed into the core, and thus decreases the time necessary to evolve to core–helium exhaustion. The correct semi-convective treatment is expected to produce a smoother composition profile outside the core. This composition profile is important in determining the structure

Downloaded from https://academic.oup.com/mnras/article/158/4/383/2603087 by guest on 26 January 2026

© Royal Astronomical Society • Provided by the NASA Astrophysics Data System

1972MNRAS.158..383D

of the helium-burning shell just after core exhaustion, and might have an appreciable effect on the model.

The author has made modifications of Paczynski's program to allow the computation of hydrogen-deficient and carbon-rich models. In addition to the abundances of hydrogen (if present), helium and carbon, the abundances of nitrogen and oxygen are explicitly determined at every mass point. The initial carbon, nitrogen, and oxygen abundances are taken to be the solar values, not the equilibrium values of the CNO cycle, in order to take advantage of existing opacity tables. Use of the higher CNO cycle abundance for nitrogen would probably have only minor effects on the convective cores of the initial models and very slight effects on the region outside the convective cores of the evolutionary models.

In the envelope integrations the first four ionization stages of carbon were included in the computation of the ionization equilibrium and in the determination of the pressure and the internal energy per gramme. Paczynski's (1969) non-iterative, summation technique was used, with the first carbon ionization considered before that of hydrogen, as the ionization potential of carbon is lower and carbon is more abundant than hydrogen in all of the computed models. The first helium and second carbon ionization potentials are nearly the same. Helium was considered first, since it is usually more abundant. The second helium ionization was considered between the third and fourth carbon ionizations.

Paczynski's program uses the Schwarzschild fitting method to construct the homogeneous main-sequence models. The program was modified to permit the construction of slightly inhomogeneous initial models, i.e. ones with a small amount of hydrogen in their atmospheres. This was accomplished by testing the temperature every time the composition was to be used. But if the temperature was greater than the specified value, the hydrogen abundance was set equal to zero and the helium abundance was increased by the amount of the hydrogen abundance. The dividing temperature was $9{\cdot}8 \times 10^6$ °K so that there would be effectively no hydrogen burning in the initial model. In Section 3 it is shown that the addition of 10^{-3} of hydrogen by mass has a negligible effect on the structure of the one-solar-mass model.

During the course of the computations of main-sequence models it was discovered that the inclusion of the N + He reaction has a noticeable effect on the conditions in the convective core and on the radius and effective temperature of the star. The numerical results are discussed in Section 3. Two sets of main-sequence models were computed, one including the N + He reaction, and the other neglecting it. It is possible to follow the evolution from the N-burning main-sequence through core nitrogen exhaustion and the establishment of core helium-burning with the triple alpha process. This was carried out only for the 1 $M_\odot$, $Z = 0{\cdot}02$ sequence of 36 models. The non-limited method of computing the boundary of the convective core must be used for these evolutionary sequences, as the convective core shrinks rapidly until nitrogen exhaustion occurs, and then expands rapidly.

To allow the inclusion of the N + He reaction without evolving the core through nitrogen exhaustion, the initial model was computed with the nitrogen reaction rate set to zero. This model had core temperature and density for the triple-alpha process. These are greater than the equilibrium values for the nitrogen reaction. The N + He reaction and the changes in the nitrogen abundance were then considered for all subsequent models. This treatment results in the nitrogen being burned out of the entire convective core between the first and second models. This

Downloaded from https://academic.oup.com/mnras/article/158/4/383/2603087 by guest on 26 January 2026

© Royal Astronomical Society • Provided by the NASA Astrophysics Data System

1972MNRAS.158..383D

treatment did not cause any convergence problems for the first evolved model. The initial nitrogen abundance was $Z_N = 0{\cdot}00092$. This evolution is further discussed in Section 3, where it is shown that all evolved models computed with this approximate method are indistinguishable from helium-burning models evolved all the way from the nitrogen-burning main sequence.

3. RESULTS

(a) *Main-sequence models*

In stars evolved from the main sequence for hydrogen-burning, the $N^{14}(\alpha, \gamma)F^{18}(e^{+}\nu)O^{18}$ reaction occurs in the contracting hydrogen-exhausted core during the ascent to the red giant tip. A small convective core develops. The core contraction is slowed until the N^{14} is exhausted, and then continues until the triple-alpha reactions ($He^4(\alpha, \gamma)Be^8(\alpha, \gamma)C^{12}$) are ignited. If evolutionary computations are to be started from the main sequence for helium-burning, the core must be evolved through nitrogen-burning, or else nitrogen-burning must be neglected.

Main sequence models with the nitrogen + helium reaction neglected were computed for 1, 2, 4 and 8 solar masses, all with $Y = 0{\cdot}98$, $Z = 0{\cdot}02$. The numerical results are summarized in Table III. The location of these models on the H–R

TABLE III

Main-sequence models for $Y = 0{\cdot}98$, $Z = 0{\cdot}02$

$M/M_\odot$	$R/R_\odot$	$\log L/L_\odot$	$\log T_e$	$\log T_c$	$\log \rho_c$	M_{cc}/M
1·0[a]	0·1994	2·3723	4·7055	8·1189	3·7727	0·2684
	0·2171	2·3676	4·6859	8·0871	3·6726	0·2760
2·0	0·3326	3·3585	4·8410	8·1697	3·3705	0·3335
	0·3619	3·3512	4·8208	8·1350	3·2622	0·3388
4·0	0·5221	4·2018	4·9539	8·2140	3·0483	0·4509
	0·5675	4·1930	4·9336	8·1755	2·9349	0·4425
8·0	0·7777	4·8986	5·0415	8·2507	2·7915	0·5968
	0·8582	4·8905	5·0181	8·2079	2·6809	0·5835

[a] For each mass, the first line pertains to the model with nirogen-burning neglected, while the second is the one with nitrogen-burning included.

diagram is indicated in Fig. 1 by the left-hand series of asterisks and the positions of the centres of these main-sequence models on the $\log \rho - \log T$ plane are shown by the upper series of asterisks in Fig. 2.

Main sequence models of the same mass and composition were also computed with the N + He reaction included. These results are summarized on alternate lines of Table III, and indicated on Figs 1 and 2. The inclusion of nitrogen-burning decreased the luminosity very slightly and shifted the main-sequence models to lower effective temperature by 0·02 in $\log T_e$. In the $\log \rho$–$\log T$ plane (Fig. 2) the nitrogen-burning models were shifted to slightly lower density (0·1 in $\log \rho_c$) and lower temperature (0·3–0·5 in $\log T_c$).

The evolution of the 1 $M_\odot$, $Z = 0{\cdot}02$ model from the main sequence for nitrogen-burning is illustrated by the solid lines in Figs 3 and 4. Nitrogen-exhaustion in the core occurred just over half-way up the loop in the H–R diagram. The convective core started to expand at this point. The tops of the loops in Figs 3 and 4

Downloaded from https://academic.oup.com/mnras/article/158/4/383/2603087 by guest on 26 January 2026

© Royal Astronomical Society • Provided by the NASA Astrophysics Data System

1972MNRAS.158..383D

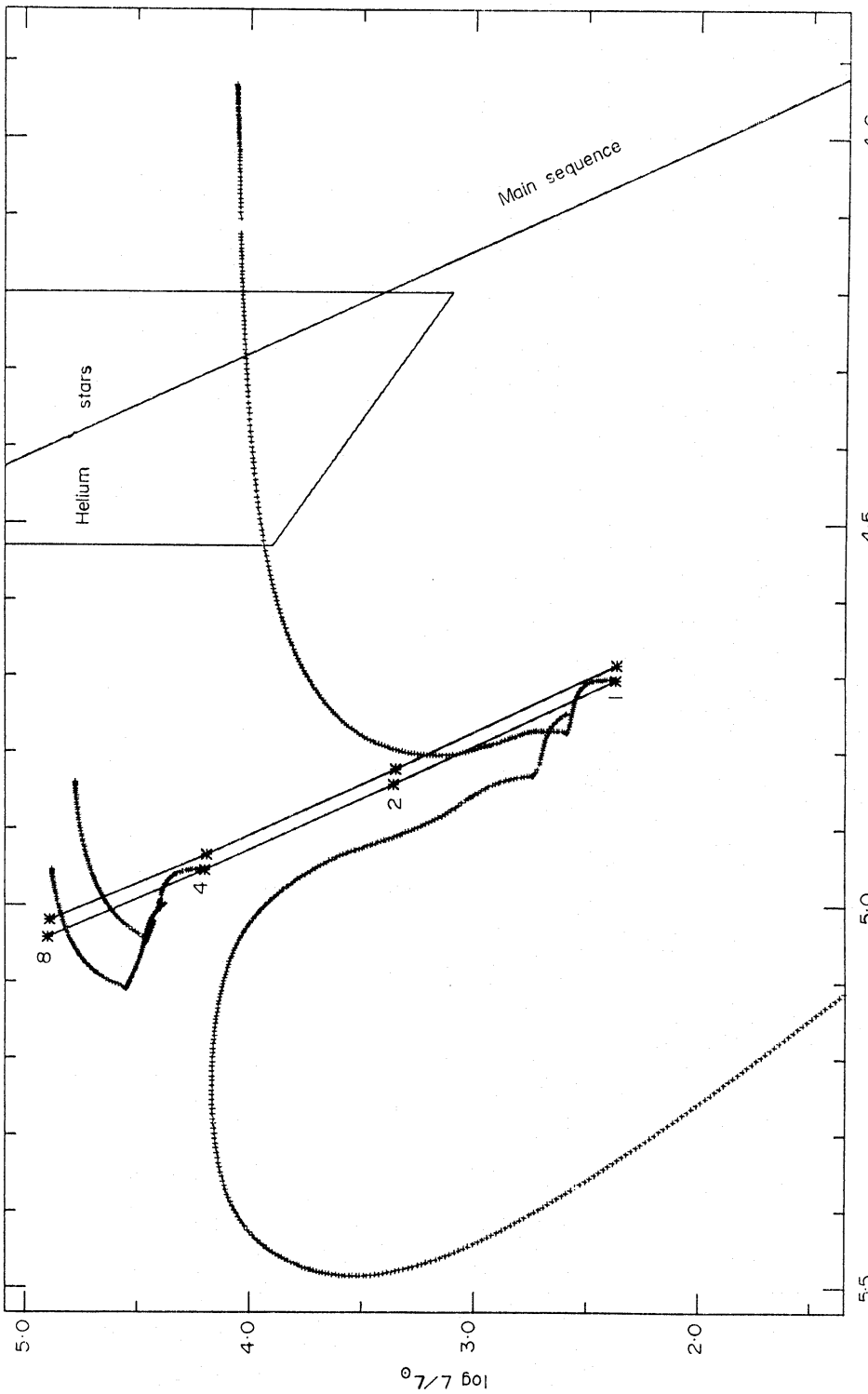

FIG. 1. *H–R diagram for main sequence and evolutionary models. The right-hand series of asterisks represents the main sequence for nitrogen-burning, while the left-hand series indicates the main sequence for helium-burning, computed with nitrogen-burning neglected. The numbers denote the masses of the models. At* 1 *and* 4 $M_\odot$, $Y = 0{\cdot}98$, $Z = 0{\cdot}02$ *was used for the lower evolutionary track and* $Y = 0{\cdot}40$, $Z = 0{\cdot}60$ *for the upper. The right-hand diagonal line represents the main sequence for hydrogen-burning. The box denotes the position of the observed extreme-helium stars, i.e. spectral types O7–B5*

Downloaded from https://academic.oup.com/mnras/article/158/4/383/2603087 by guest on 26 January 2026

© Royal Astronomical Society • Provided by the NASA Astrophysics Data System

1972MNRAS.158..383D

correspond to the phase of maximum density in the convective core. The central temperature increased slowly, and then was constant for the last half of the decrease in luminosity. The expansion of the convective core halted just before the luminosity minimum; the position of the core stabilized in the fourth model after the

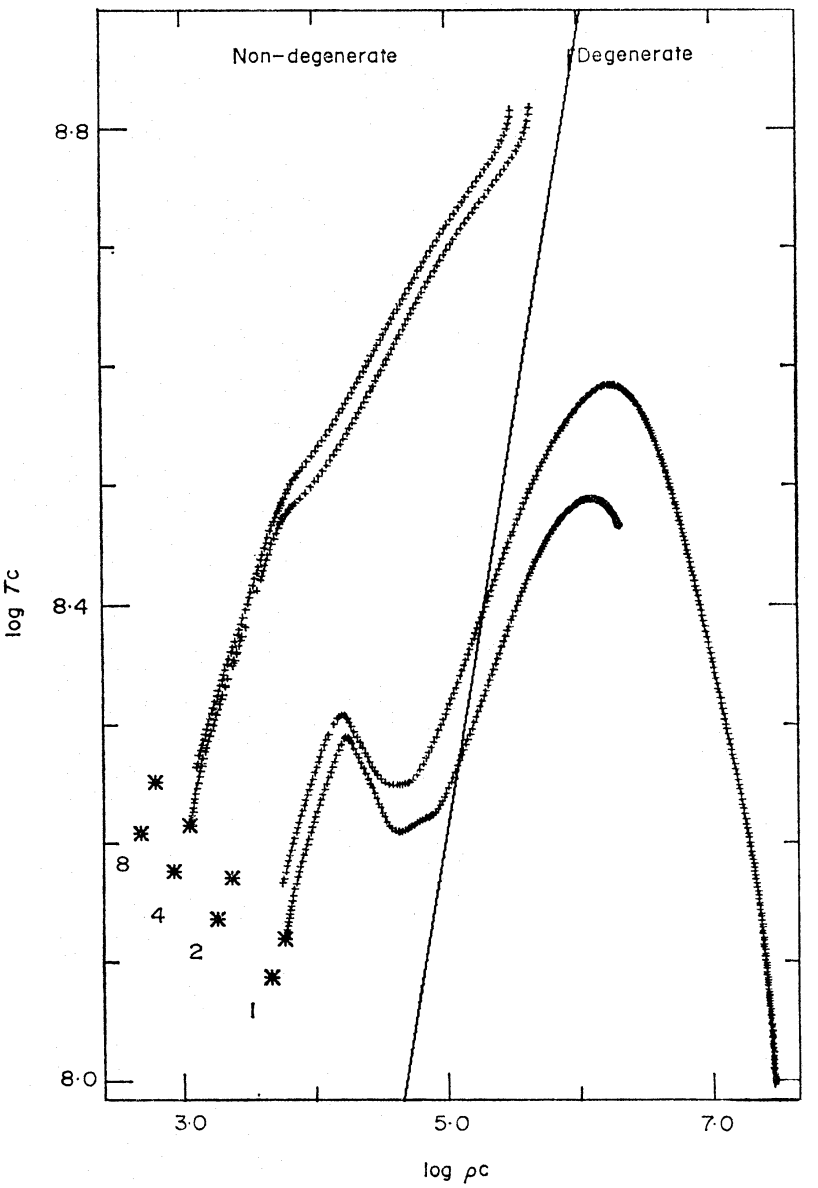

FIG. 2. *Log* T_c *versus log* ρ_c *for main-sequence and evolutionary models. The lower series of asterisks represents the main sequence for nitrogen-burning, while the upper indicates the main sequence for helium-burning, computed with nitrogen-burning neglected. The numbers denote the masses of the models. At both* 1 *and* 4 $M_\odot$, $Z = 0{\cdot}02$ *was used for the lower evolutionary track and* $Z = 0{\cdot}60$ *for the upper. The diagonal line indicates the conditions at which the degenerate and non-degenerate formulae give the same electron pressure.*

minimum. The central temperature and luminosity increased rapidly after the luminosity minimum, which should be regarded as the correct main-sequence model for helium-burning. At this point the radius of the star, which had been decreasing since the first model, began the steady increase that is characteristic of evolution off the main sequence.

Downloaded from https://academic.oup.com/mnras/article/158/4/383/2603087 by guest on 26 January 2026

© Royal Astronomical Society • Provided by the NASA Astrophysics Data System

1972MNRAS.158..383D

The asterisks on Figs 3 and 4 indicate the positions of the main-sequence model that was computed with the N + He reaction neglected, and of the first 14 evolved models. It can be seen that the luminosity and the central density of the initial model are slightly lower than those for the correct main-sequence model, but that

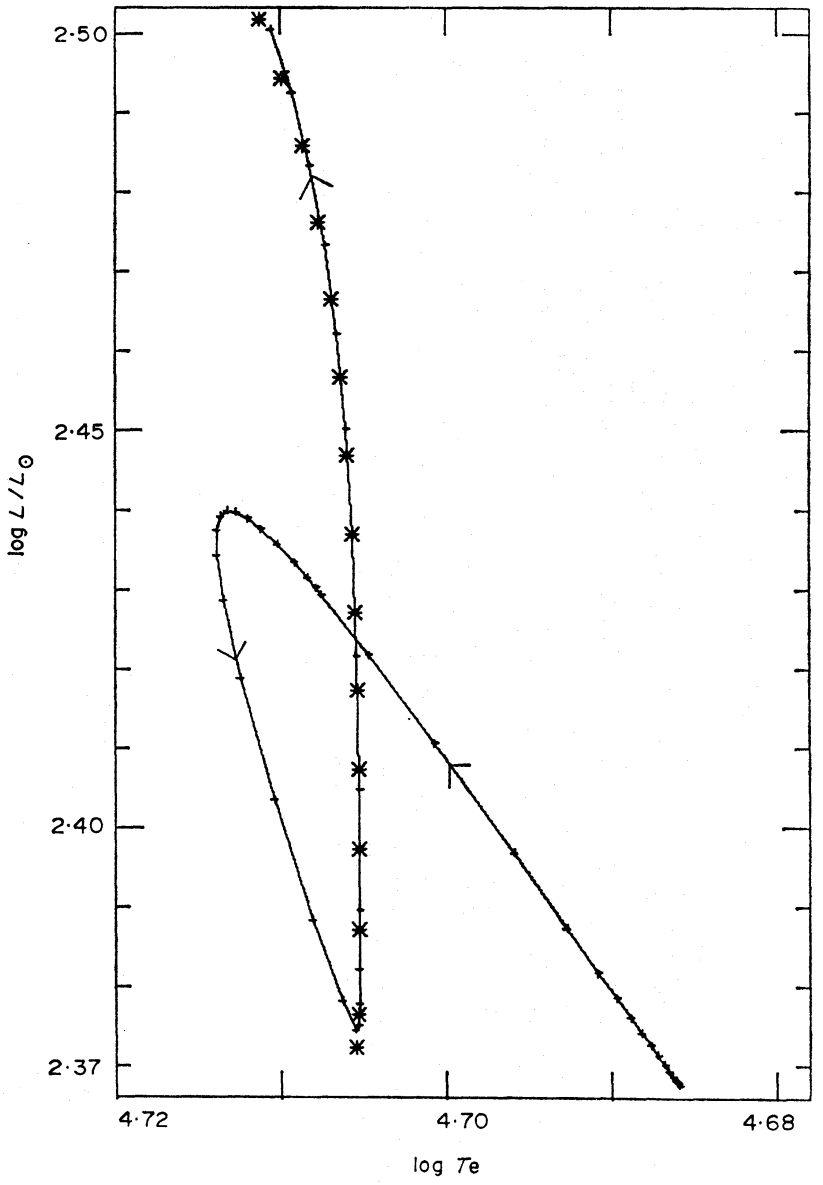

FIG. 3. *H–R diagram for the evolution of the* 1 $M_\odot$ *model from the main sequence for nitrogen-burning. The solid line represents the evolution from the main sequence for nitrogen-burning through core nitrogen exhaustion to the main sequence for helium-burning and the subsequent evolution off the latter main sequence. The asterisks indicate the first* 15 *models computed with the approximate scheme described in Section* 2.

the evolved models fall on the lines determined by the evolution from the main sequence for nitrogen-burning. It was concluded that the approximate method for the computation of the main sequence model, which was described in Section 2, could be used without any hesitation, since the approximate model was so similar to the minimum luminosity model of the sequence that had been evolved through nitrogen-burning.

Downloaded from https://academic.oup.com/mnras/article/158/4/383/2603087 by guest on 26 January 2026

© Royal Astronomical Society • Provided by the NASA Astrophysics Data System

1972MNRAS.158..383D

The two sequences of evolutionary models eventually diverged, due to the different treatment of the boundary to the convective core. The non-limited method was used for the sequence that started from the main-sequence for nitrogen-burning, while the method with the limited core expansion was used for the evolution from the main sequence for helium-burning. At the luminosity minimum, defined

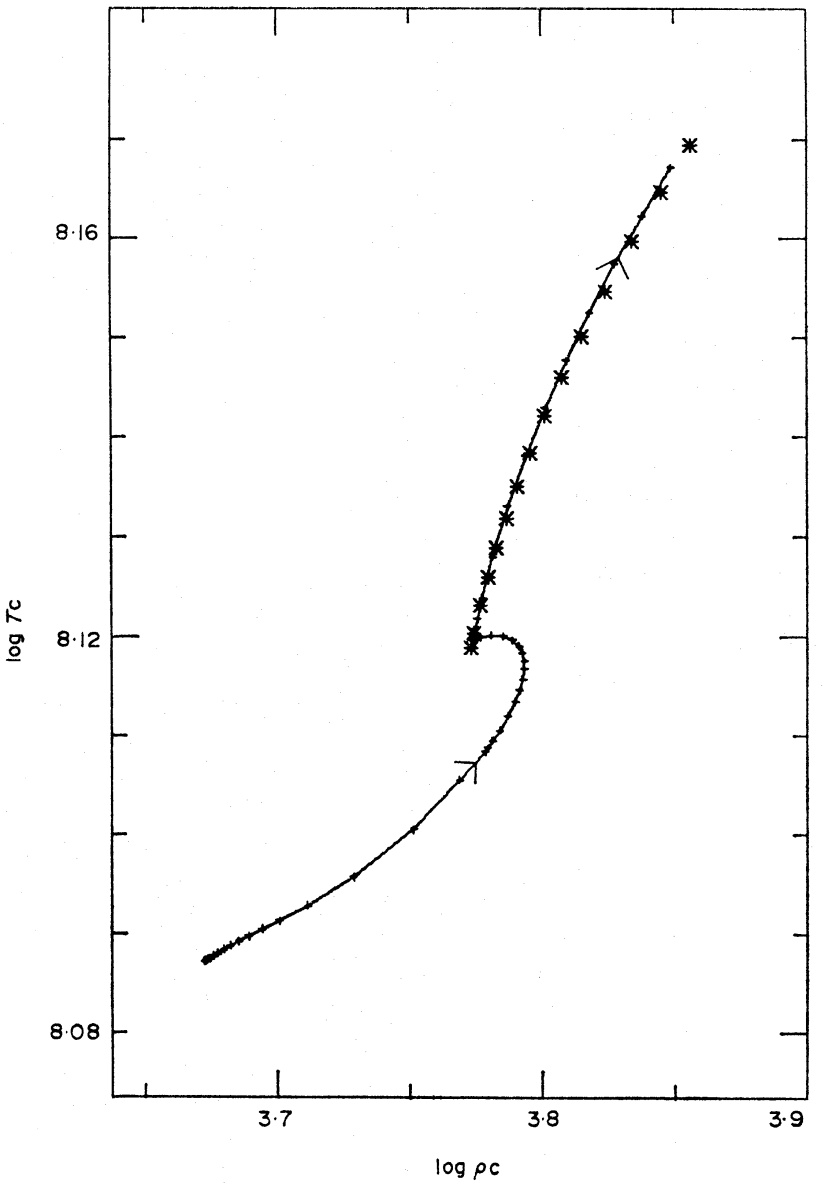

FIG. 4. *Log* T_c *versus log* ρ_c *for the evolution of the* 1 $M_\odot$ *model from the main sequence for nitrogen-burning. The symbols should be interpreted as in Fig.* 3.

to be the correct main sequence model for helium-burning, the convective core of the model that had been evolved through core–nitrogen exhaustion was larger than the core of the initial model on the main sequence for helium-burning by 0·006 $M_\odot$. The cores of both sequences expanded slightly and were then steady in mass fraction until the problem with semi-convection occurred, which caused the convective core of the model evolved through nitrogen-burning to expand. The mixing slowed the helium depletion in the core, thereby slowing the increase in

© Royal Astronomical Society • Provided by the NASA Astrophysics Data System

Downloaded from https://academic.oup.com/mnras/article/158/4/383/2603087 by guest on 26 January 2026

1972MNRAS.158..383D

central temperature and density and causing the two sequences of the model to diverge.

The upper limit on the hydrogen abundance in the extreme-helium stars is 10^{-3} by mass. In order to test the effect of this amount of hydrogen on the stellar models, the 1 $M_\odot$ main-sequence model with nitrogen-burning included was recomputed with 10^{-3} of hydrogen added to all the zones of the model in which the temperature was less than $9{\cdot}8 \times 10^6$ °K. The two models are compared in Table IV.

TABLE IV

Effect of hydrogen on 1 $M_\odot$, nitrogen-burning model

X	$R/R_\odot$	$\log L/L_\odot$	$\log T_e$	$\log T_c$	$\log \rho_c$	M_{cc}/M
0·0	0·21705	2·3676	4·6859	8·0871	3·6726	0·275985
0·001	0·21716	2·3676	4·6858	8·0871	3·6726	0·276021

There was no change in the temperature as a function of mass between the two models, but the density was slightly greater throughout the convective core of the model with the hydrogen-enriched envelope. The value of $\log \rho_c$ increased by 0·000007. This greater density resulted in a slightly larger convective core. Outside the core the density gradient was steeper in the hydrogen-enriched model. The hydrogen enrichment lowered the effective temperature and density of the outer envelope of the star, and caused the radius of the star to increase. Since these differences were all considered to be negligible, no more hydrogen-enriched models were computed.

The effect of the enrichment with carbon on the 1 $M_\odot$, non-nitrogen-burning main-sequence model is summarized in Table V. The carbon enrichment produced

TABLE V

Effect of additional carbon

			1 $M_\odot$			
Z	$R/R_\odot$	$\log L/L_\odot$	$\log T_e$	$\log T_c$	$\log \rho_c$	M_{cc}/M
0·02	0·19941	2·3723	4·7055	8·1189	3·7727	0·268411
0·04	0·19976	2·3709	4·7048	8·1199	3·7692	0·267673
0·08	0·20156	2·3824	4·7057	8·1223	3·7656	0·266827
0·16	0·20377	2·4078	4·7097	8·1273	3·7583	0·262931
0·32	0·20717	2·4670	4·7209	8·1387	3·7474	0·258531
0·60	0·20817	2·5902	4·7507	8·1654	3·7446	0·266688
			4 $M_\odot$			
Z	$R/R_\odot$	$\log L/L_\odot$	$\log T_e$	$\log T_c$	$\log \rho_c$	M_{cc}/M
0·02	0·52209	4·2018	4·9539	8·2140	3·0483	0·450889
0·60	0·51478	4·3712	4·9993	8·2631	3·0878	0·495641

an increased opacity in the atmosphere, which caused the outer layers of the star to expand. However, because of the higher central temperature and greater nuclear reaction rates, a large carbon abundance also increased the luminosity of the star. Since the luminosity rose faster than R^2, the effective temperature of the star also increased, as $L = 4\pi R^2 \sigma T_e^4$.

The behaviour of the luminosity of the $Z = 0{\cdot}04$ (0·02 extra carbon) and $Z = 0{\cdot}08$ (0·06 extra carbon) models was unusual. Even though the central temperature and density changes fell along the smooth curve applicable to all the carbon

Downloaded from https://academic.oup.com/mnras/article/158/4/383/2603087 by guest on 26 January 2026

© Royal Astronomical Society • Provided by the NASA Astrophysics Data System

1972MNRAS.158..383D

enrichments, the luminosity decreased very slightly between $Z = 0{\cdot}02$ and $0{\cdot}04$, and then rose slightly between $Z = 0{\cdot}04$ and $0{\cdot}08$ (see Table V). The small enhancement in the temperature of the core was offset by the decreasing density and helium abundance; the energy production of the triple-alpha process fell. The greater carbon abundance amplified the energy production of the $C^{12}+He$ reaction, but this was not enough to counteract the decrease in the amount of energy produced by the triple-alpha process, so the total energy production declined. As the carbon abundance rose further, the $C^{12}+He$ reaction was able to supply more energy, and the total luminosity increased. The variation in the effective temperature reflected this variation in the luminosity.

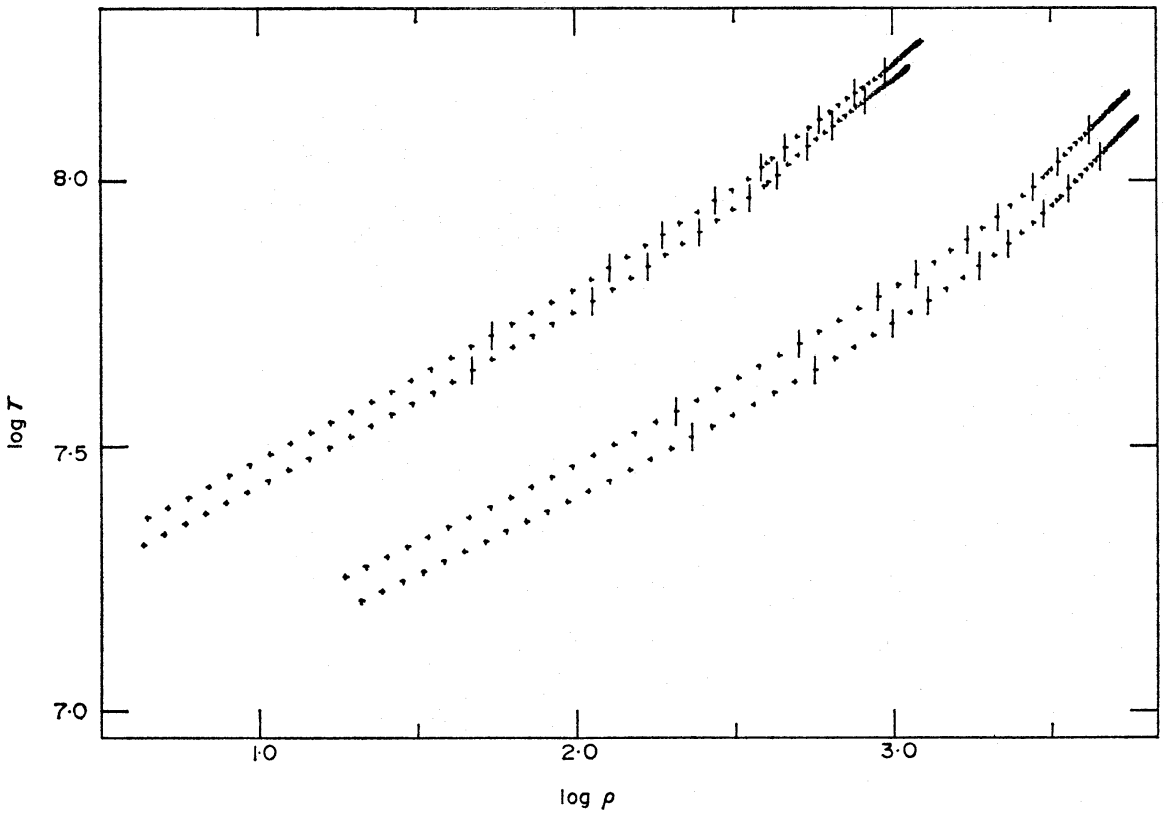

FIG. 5. *Log* T *versus log* ρ *Profiles for* 1 *and* 4 M$_\odot$ *models, each for* Z = 0·02 *and* Z = 0·60. *The upper curves are for* 4 M$_\odot$, *the lower for* 1 M$_\odot$. *At each mass, the upper curve corresponds to* Z = 0·60, *the lower to* Z = 0·02. *The short vertical lines indicate the location of tenths of the mass fraction.*

A $4\,M_\odot$, $Z = 0{\cdot}60$ main-sequence model was also computed. The important properties of this model are listed in Table V. The relationship between the $Z = 0{\cdot}02$ and $0{\cdot}60$ $4\,M_\odot$ models was somewhat different than that between the two $1\,M_\odot$ models of the same compositions. The profiles of these four models in the log ρ–log T plane are illustrated in Fig. 5. As at $1\,M_\odot$, the energy production in the $4\,M_\odot$ models was less concentrated to the centre of the star at $Z = 0{\cdot}60$. However, the radiative temperature gradient was not as steep and the convective core was approximately 10 per cent larger at $Z = 0{\cdot}60$ than at 0·02, even though at $1\,M_\odot$ the convective core had been slightly smaller at $Z = 0{\cdot}60$ than at 0·02. From Fig. 5 one can see that the temperature at a given mass fraction was always greater for the carbon-enriched model than for the unenriched model of the same

Downloaded from https://academic.oup.com/mnras/article/158/4/383/2603087 by guest on 26 January 2026

© Royal Astronomical Society • Provided by the NASA Astrophysics Data System

1972MNRAS.158..383D

mass. The carbon enrichment increased the density at a given mass fraction in the 4 $M_\odot$ models and decreased it in the 1 $M_\odot$ models. The carbon enrichment from $Z = 0{\cdot}02$ to $0{\cdot}60$ produced an increase of about 11 per cent in the effective temperature for both masses. The luminosity increased by approximately 65 per cent at 1 $M_\odot$ and 48 per cent at 4 $M_\odot$.

(b) *Evolutionary models*

The important phases of the evolution of the 1 $M_\odot$, $Z = 0{\cdot}02$ model are listed in Table VI. The profiles of these selected evolutionary models in the log ρ–log T plane are shown in Fig. 6. The evolutionary tracks on the H–R diagram and in the log ρ_c–log T_c plane are illustrated in Figs 1 and 2, respectively. The initial rise off the main sequence was followed by a curve toward higher effective temperature when the helium-exhaustion in the core forced the entire star to contract.

TABLE VI

Evolution at one solar mass, $Z = 0{\cdot}02$

Phase	$R/R_\odot$	$\log L/L_\odot$	$\log T_e$	$\log T_c$	$\log \rho_c$	L_{core}/L	Time (10^6 yr)
Main sequence	0·2005	2·3722	4·7055	8·1189	3·7737	0·0000	0
Core helium exhaustion	0·2138	2·6987	4·7730	8·2408	4·4418	0·0000	8·0818
Initial shell-burning	0·2974	3·1099	4·8042	8·2640	5·0658	0·0133	9·9140
Shell-burning	0·5449	3·5196	4·7751	8·4025	5·5340	0·0387	10·5519
Temperature inversion	7·6734	4·0082	4·3230	8·4812	6·0273	0·0749	10·8119

The abrupt change to rising luminosity at nearly constant effective temperature occurred when the central helium content had decreased to $Y_c = 0{\cdot}00282$. The general contraction of the star ended at this time and a rapid expansion began as the effective energy generation switched to a shell outside the shrinking convective core. The maximum central temperature (see Fig. 2) also occurred at this phase. The nearly helium-exhausted core contracted and cooled as it released thermal energy.

The minimum in the central temperature and the final exhaustion of helium in the core occurred halfway between the sharp hook in the track and the second crossing of the main sequence for helium-burning. The final abundance in the $0{\cdot}229\ M_\odot$, helium-exhausted core were $Z_C = 0{\cdot}625$, $Z_O = 0{\cdot}367$. At this phase the gravitational contraction of the core supplied 1·2 per cent of the total luminosity of the star. The thick helium-burning shell that extended from $M_r/M = 0{\cdot}570$ to 0·797 produced 90 per cent of the luminosity.

As the evolution proceeded the gravitational contraction of the growing helium-exhausted core contributed a larger fraction of the total luminosity. The rising degeneracy and the resultant plasma neutrino emission produced a temperature inversion in the core when its mass reached $0{\cdot}596\ M_\odot$ and the central density was $\log \rho_c = 5{\cdot}96$. The temperature inversion forced the luminosity of all regions inside the temperature maximum to become negative; these zones absorbed energy from the outer parts of the core, since they were emitting more energy via plasma neutrinos than the gravitational contraction could supply. The maximum temperature rose slowly as the point of highest temperature moved steadily out from the centre of the star, staying near the mass shell where $\log \rho_c = 5{\cdot}78$, which was the effective threshold for plasma neutrino emission.

Downloaded from https://academic.oup.com/mnras/article/158/4/383/2603087 by guest on 26 January 2026

© Royal Astronomical Society • Provided by the NASA Astrophysics Data System

1972MNRAS.158..383D

On the H–R diagram (Fig. 1) the phase of shell-burning a highly degenerate, neutrino-emitting core is characterized by nearly horizontal evolution toward lower effective temperatures. The present evolutionary sequence entered the region of the observed extreme-helium stars at log $T_e = 4{\cdot}53$, or spectral type O7, with log $L/L_\odot = 3{\cdot}93$, $M_{bol} = -5{\cdot}09$, $M_V \approx -1{\cdot}5$. It crossed the main sequence for hydrogen-burning at log $T_e = 4{\cdot}32$, spectral class B1–B2, with log $L/L_\odot = 4{\cdot}01$, $M_{bol} = -5{\cdot}34$, $M_V \approx -3$. The evolutionary track left the region of the observed stars at log $T_e = 4{\cdot}2$, or spectral type B5, with log $L/L_\odot = 4{\cdot}03$, $M_{bol} = -5{\cdot}34$,

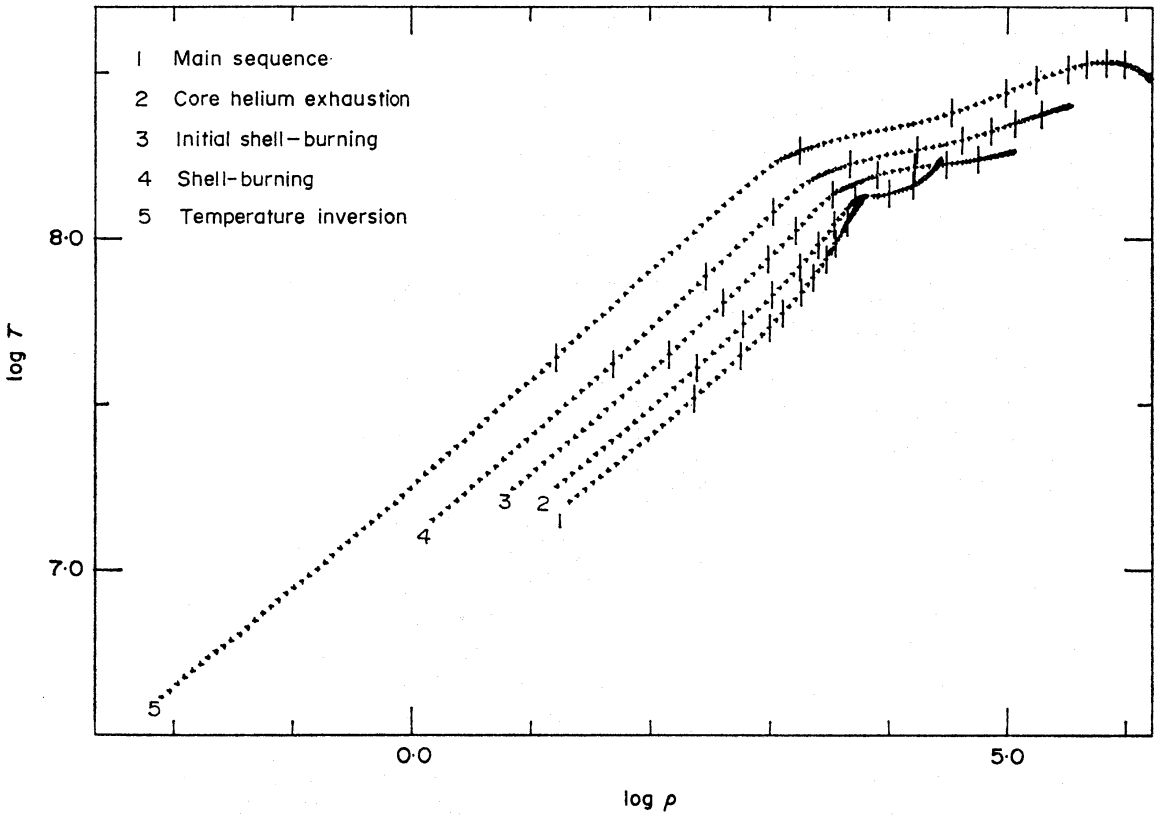

FIG. 6. *Log* T *versus log* ρ *profiles for selected evolutionary models of* 1 $M_\odot$, Z = 0·02. *The numbers denote the tracks in the order of Table VI. The short vertical lines indicate the location of tenths of the mass fraction.*

$M_V \approx -3{\cdot}9$. The evolutionary time across the area of the H–R diagram occupied by the extreme-helium stars was 3500 yr. The temperature inversion model listed in Table VI and shown in Fig. 6 is the one that was closest to the main sequence for hydrogen-burning. The evolutionary computations of the 1 $M_\odot$, $Z = 0{\cdot}02$ sequence were stopped when the rapid changes in the outer layer of the star had forced the time step between models to be less than 100 yr.

The evolution of the 1 $M_\odot$, $Z = 0{\cdot}60$ model is indicated in Figs 1 and 2. The conditions at the important evolutionary phases are listed in Table VII. Fig. 7 illustrates the profiles of these models in the log ρ–log T plane. From Fig. 2 it can be seen that the evolution of the core closely resembled that of the 1 $M_\odot$, $Z = 0{\cdot}02$ model. The evolutionary time scale was faster by a factor of 2–3 for the $Z = 0{\cdot}60$ sequence, primarily because there was less nuclear fuel to burn. The similar evolution resulted from the fact that $Y = 0{\cdot}40$, $Z_C = 0{\cdot}58$ was not an

Downloaded from https://academic.oup.com/mnras/article/158/4/383/2603087 by guest on 26 January 2026

© Royal Astronomical Society • Provided by the NASA Astrophysics Data System

1972MNRAS.158..383D

TABLE VII

Evolution at one solar mass, $Z = 0{\cdot}60$

Phase	$R/R_\odot$	$\log L/L_\odot$	$\log T_e$	$\log T_c$	$\log \rho_c$	L_{core}/L	Time (10^6 yr)
Main sequence	0·2082	2·5902	4·7606	8·1654	3·7446	0·0000	0
Core helium exhaustion	0·1844	2·8213	4·8348	8·2801	4·3461	0·0000	2·7631
Initial shell-burning	0·2093	3·0981	4·8764	8·2706	4·8271	0·0270	3·3364
Shell-burning	0·2621	3·4848	4·9243	8·4069	5·3128	0·0577	3·7958
Temperature inversion	0·1770	4·1563	5·1774	8·5569	6·4920	0·2060	4·1083
White dwarf	0·0085	0·0681	4·8142	7·9033	7·4763	0·2167	4·7719

unusual composition for a helium-burning convective core. In both sequences of models, the triple-alpha process raised the central carbon abundance to nearly 75 per cent by mass before the $C^{12}+He$ reaction depleted the carbon. Thus the core of the initial $Z = 0{\cdot}60$ model closely resembled the core of an evolved $Z = 0{\cdot}02$ model. Major differences occurred only in the region outside the convective core, where nuclear reactions had produced a composition profile quite different from that of the $Z = 0{\cdot}02$ model.

The mass of the helium-exhausted core increased much more rapidly at $Z = 0{\cdot}60$, as the burning shell was hotter and had less fuel to process. Since the temperature was higher, degeneracy did not become important in the $Z = 0{\cdot}60$ model until later in the evolution than it had at $Z = 0{\cdot}02$. The central temperature inversion appeared when the mass of the helium-exhausted core was $0{\cdot}711\ M_\odot$. After this the entire model contracted. At the point of maximum temperature,

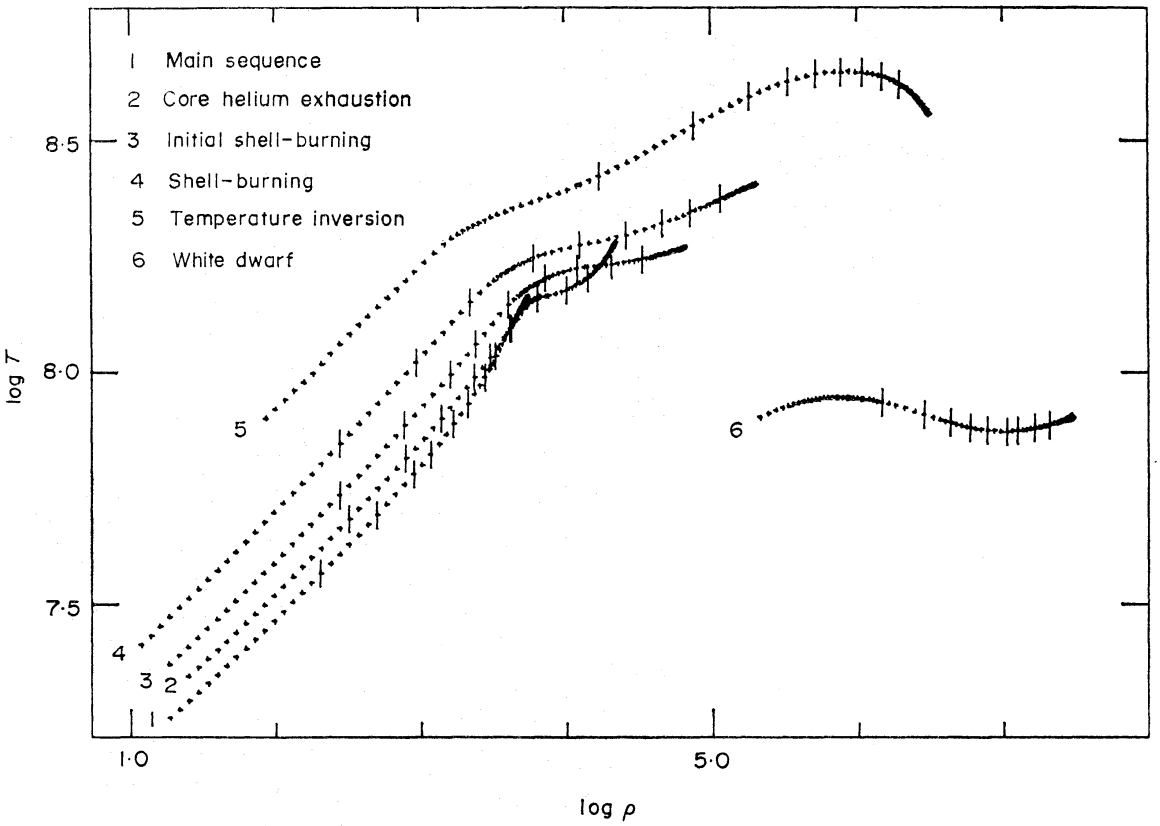

FIG. 7. *Log* T *versus log* ρ *profiles for selected evolutionary models of* 1 $M_\odot$, $Z = 0{\cdot}60$. *For the data of Table VII, the numbers and symbols should be interpreted as in Fig.* 6.

Downloaded from https://academic.oup.com/mnras/article/158/4/383/2603087 by guest on 26 January 2026

© Royal Astronomical Society • Provided by the NASA Astrophysics Data System

1972MNRAS.158..383D

which moved away from the centre of the star, log ρ rose from 5·82 to 6·10 and then remained near this density as the maximum temperature decreased. The mass of the helium-exhausted core had reached 0·985 $M_\odot$ by the time the maximum temperature of log T = 8·58 had occurred at M_r/M = 0·684.

After the occurrence of maximum temperature the entire star cooled rapidly, with the central density increasing only slowly as it approached log ρ_c = 7·5. When the conditions in the centre reached log T_c = 8·083, log ρ_c = 7·403 the diminished efficiency of the plasma neutrino process caused the region of negative luminosity to move outward, toward lower density. Even though the central temperature continued to decline from model to model, the temperature decreased outward from the centre to the region of negative luminosity, where the temperature inversion occurred.

The computations were halted when the helium-burning shell had been extinguished and the model was approaching contraction at a constant radius. If followed further, the model would simply have continued to cool, since it was well below the core mass of 1·37 $M_\odot$ required for carbon ignition (Arnett 1968, 1969; Rose 1969).

In spite of the fact that the evolution of the core of the Z = 0·60 model showed little qualitative difference from the evolution at Z = 0·02, the tracks on the H–R diagram (Fig. 1) were quite different. The initial rise in luminosity off the main sequence was smaller at Z = 0·60. since the core helium was already partially exhausted. The hook toward rapidly rising luminosity, which occurred when the radius reached a minimum, was not quite as sharp as at Z = 0·02, but was still similar. The two tracks remained roughly parallel as long as the evolution of the star was governed by the conditions in the convective or helium-exhausted core. But, once the helium-burning shell dominated the evolution, the two sequences of models diverged, since the shell structures were quite different. The Z = 0·60 models had much thinner and hotter shells that moved outward more rapidly, and hotter and more dense envelopes. Because of the smaller luminosity increase and shorter time-scale, the helium-burning shell did not supply enough energy to force the stellar envelope to expand. The Z = 0·60 model contracted and evolved toward higher effective temperature, while the one for Z = 0·02 expanded and evolved toward lower effective temperature. The later crossed the region of the observed stars and became a giant, while the carbon-rich model became a hot white dwarf and never approached the region of the observed stars.

At 4 $M_\odot$ there were no qualitative differences between the evolutionary tracks for Z = 0·02 and Z = 0·60. The conditions at the important phases of evolution of these models are given in Tables VIII and IX. The profiles of selected 4 $M_\odot$, Z = 0·60 models in the log ρ–log T plane are illustrated in Fig. 8. Relative to the Z = 0·02 models, the Z = 0·60 evolutionary tracks were simply shifted to higher

TABLE VIII

Evolution at four solar masses, Z = 0·02

Phase	$R/R_\odot$	log $L/L_\odot$	log T_e	log T_c	log ρ_c	L_{core}/L	Time (10^6 yr)
Main sequence	0·3326	3·3585	4·8410	8·1697	3·3705	0·0000	0
Core helium exhaustion	0·4674	4·4417	5·0390	8·4454	3·6591	0·0000	1·0817
Shell-burning	0·9493	4·7081	4·9506	8·6394	4·7174	0·2740	1·1183
After carbon ignition	1·7025	4·7725	4·8405	8·8212	5·6378	0·3475	1·1337

Downloaded from https://academic.oup.com/mnras/article/158/4/383/2603087 by guest on 26 January 2026

© Royal Astronomical Society • Provided by the NASA Astrophysics Data System

1972MNRAS.158..383D

TABLE IX

Evolution at four solar masses, Z = 0·60

Phase	$R/R_\odot$	$\log L/L_\odot$	$\log T_e$	$\log T_c$	$\log \rho_c$	L_{core}/L	Time (10^5 yr)
Main sequence	0·5148	4·3711	4·9993	8·2631	3·0878	0·0000	0
Core helium exhaustion	0·3999	4·5117	5·0892	8·4560	3·6448	0·0000	3·6274
Shell-burning	0·5825	4·7508	5·0673	8·6118	4·4609	0·3041	3·8668
Before carbon ignition	1·1027	4·8745	4·9597	8·7986	5·4491	0·3698	4·0492
After carbon ignition	1·1368	4·8777	4·9539	8·8199	5·4950	0·3896	4·0535

central temperature and density (see Fig. 2) and greater luminosity and effective temperature (see Fig. 1). The initial rise off the main sequence was followed by a hook to higher effective temperature as the radius decreased. The minimum in radius occurred just after core helium-exhaustion; the models then evolved along smooth and nearly parallel curves toward higher luminosity and lower effective temperature until carbon ignition took place at the centre of the helium-exhausted cores. Both models were then approaching the end of the phase of helium-burning in a thick shell.

4. RESULTS OF OTHER INVESTIGATORS

L'Ecuyer's (1966) 0·7 $M_\odot$ model evolved directly to the white dwarf region, while Osaki's (1963) 0·8 $M_\odot$ model appeared to be evolving toward lower effective temperatures when his computations stopped. Models of approximately 0·8 to

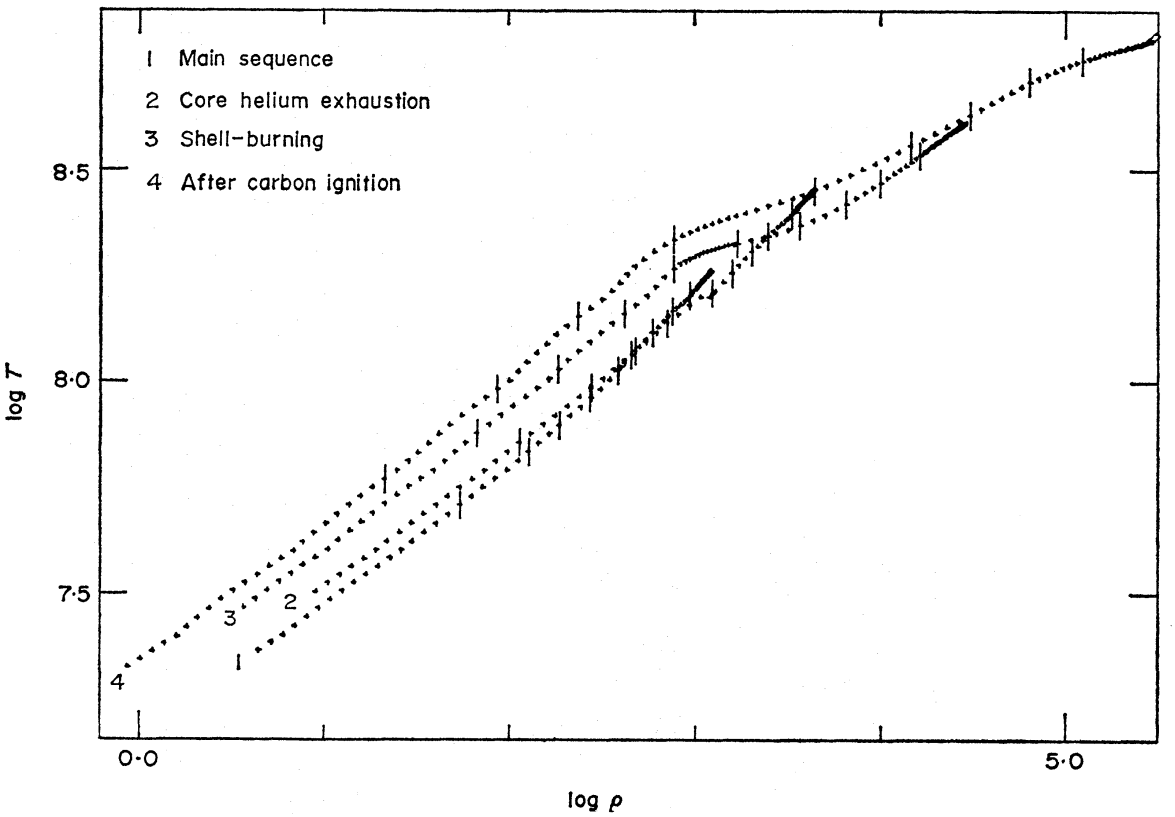

FIG. 8. *Log* T *versus log* ρ *profiles for selected evolutionary models of* 4 $M_\odot$, Z = 0·60. *For the data of Table IX, the numbers and symbols should be interpreted as in Fig.* 6.

Downloaded from https://academic.oup.com/mnras/article/158/4/383/2603087 by guest on 26 January 2026

© Royal Astronomical Society • Provided by the NASA Astrophysics Data System

1972MNRAS.158..383D

$1{\cdot}4\,M_\odot$ should evolve toward the red giant region of the H–R diagram, and then rapidly return to higher effective temperatures as their helium-burning shells are extinguished. These models are not massive enough to ignite carbon.

Above $1{\cdot}4\,M_\odot$ ($M_{\rm core} \geq 1{\cdot}37\,M_\odot$), carbon will ignite in the core, but under highly explosive, degenerate conditions in the stars of lower mass (Arnett 1968, 1969; Rose 1969). Helium stars with $1{\cdot}4 \leq M/M_\odot \leq 4{\cdot}0$ should evolve to lower effective temperatures at least until carbon ignition occurs. Stars near the middle of this mass range, $M \approx 2$ to $3\,M_\odot$, would probably ignite carbon while they were near the region of the observed helium stars.

It is possible that some or all of the observed extreme helium stars are evolving to the left in the H–R diagram, rather than to the right as the models computed in the present work did. They could either be stars that were once on the main sequence for helium-burning and are now returning from the red giant region, or ones like Paczynski's (1970a) models that lost their hydrogen-rich envelopes in the red giant region and rapidly evolved to the white dwarf state. Paczynski's models evolved at constant luminosity until the helium shell source burned out, and then cooled to white dwarfs. His models of 0·6, 0·8 and $1{\cdot}2\,M_\odot$ had $\log L/L_\odot = 3{\cdot}67$, $4{\cdot}21$ and $4{\cdot}60$ and crossed the region of the observed helium stars in times of approximately 4000, 80 and 3 yr, respectively.

5. CONCLUSIONS

The possibility that the observed extreme helium stars are evolving from the helium-burning main sequence to the right in the H–R diagram has been investigated. During the phase of helium-burning in a shell surrounding a highly degenerate carbon–oxygen core $1\,M_\odot$ stars with an initial composition of 98 per cent helium do evolve left to right across the region of the H–R diagram occupied by the observed helium stars. In contrast, $1\,M_\odot$ stars with an initial carbon abundance of 58 per cent evolve toward the white dwarf region without ever approaching the region of the observed helium stars. At $4\,M_\odot$ the initial carbon abundance has no qualitative effect on the evolution; stars of both initial compositions evolve to the right in the H–R diagram. These stars were approaching the region of the observed helium stars when carbon ignited in their cores under non-degenerate conditions. Their evolution was not followed further, but the $4\,M_\odot$ stars of both compositions will cross the region of the observed helium stars if their evolution at nearly constant luminosity is not greatly altered after carbon ignition. Although carbon-burning models were not included in the present computations, it is expected that core carbon burning is the slowest evolutionary phase for which stars without hydrogen could be in the region of the H–R diagram occupied by the observed extreme-helium stars.

Hunger & Klinglesmith (1969) derived $X = 0{\cdot}001$, $Y = 0{\cdot}45$ and $Z = 0{\cdot}55$ for BD+10° 2179, and used the luminosity estimate of $M_V \leq -1{\cdot}6$ to derive $M \geq 0{\cdot}5\,M_\odot$, $R \geq 4{\cdot}6\,R_\odot$. From the present work it is concluded that unless BD+10°2179 is rapidly contracting and evolving to the left on the H–R diagram, it is more massive than $1\,M_\odot$. If it was ever near the main sequence for helium-burning, it has $M > 1\,M_\odot$. Using Hunger & Klinglesmith's values of $\log g = 2{\cdot}8$, $\log T_e = 4{\cdot}2$, if $M > 1\,M_\odot$, $R > 6{\cdot}2\,R_\odot$, $M_{\rm bol} < -3{\cdot}5$, and $M_V < -2{\cdot}2$.

It is not possible to make meaningful estimates of the actual abundances of extreme-helium stars as the number of known examples is very small and the

Downloaded from https://academic.oup.com/mnras/article/158/4/383/2603087 by guest on 26 January 2026

© Royal Astronomical Society • Provided by the NASA Astrophysics Data System

1972MNRAS.158..383D

masses, luminosities, and origins are not known. Since the extreme-helium stars seem to be relatively rare, the short times that the computed models spend in the region of the observed stars are not necessarily evidence that the models are incorrect.

Helium stars of many different masses could cross the region of interest from right to left during the contraction to the white dwarf state that would follow the loss of the hydrogen-rich envelope in the red-giant region. The time scale would depend on the mass and composition, and would be shorter for the more massive stars.

The time necessary for a given star to transverse the area of the observed stars is of the order of a few thousand years in the most advantageous cases, and is often much shorter. Since the helium-star models computed here and elsewhere evolve at essentially constant luminosity when they are near the main sequence for hydrogen-burning, no correlation between the luminosity and spectral type of a helium star can be expected. The luminosity depends on the mass and composition, while the effective temperature is determined by the state of evolution.

ACKNOWLEDGMENTS

The author is extremely indebted to her faculty advisor, Dr Laura P. Bautz, for her continued advice and encouragement. Drs John D. Bahng and William Buscombe have made a number of helpful comments. Drs Cox and Stewart and their colleagues at Los Alamos are to be thanked for their gracious computation of the opacity tables that made this work possible. Throughout the course of this work the author was supported by a fellowship from the Graduate School of Northwestern University. Northwestern University also furnished generous amounts of computer time for these computations. This assistance is gratefully acknowledged.

Astronomy Department, Northwestern University, Evanston, Illinois 60201

Present address:
University of Wisconsin, Eau Claire, Wisconsin 54701

Received in original form 1971 *September* 1

REFERENCES

Aller, L. H., 1959. *Modeles d'etoiles et evolution stellaire*, p. 41, extrait des Memoires in −8° de la Societe Royale des Sciences des Liege, Cinquieme Series, T. 3.
Auman, J., 1967. *Astrophys. J. Suppl.*, **14**, 171.
Arnett, W. D., 1968. *Nature*, **219**, 1344.
Arnett, W. D., 1969. *Astrophys. Space Sci.*, **5**, 180.
Beaudet, G., Petrosian, V. & Salpeter, E. E., 1967. *Astrophys. J.*, **150**, 979.
Canuto, V., 1970. *Astrophys. J.*, **159**, 641.
Cox, A. N. & Stewart, J. N., 1969. Sci. Inf. of the Astron. Council, *USSR Academy of Sciences*, vol. 15.
Cox, J. P. & Giuli, R. T., 1961. *Astrophys. J.*, **133**, 755.
Cox, J. P. & Salpeter, E. E., 1961. *Astrophys. J.*, **133**, 764.
Cox, J. P. & Salpeter, E. E., 1964. *Astrophys. J.*, **140**, 485.
Crawford, J. A., 1953. *Publ. astr. Soc. Pacific*, **65**, 210.
Deinzer, W. & Salpeter, E. E., 1964. *Astrophys. J.*, **140**, 499.

Downloaded from https://academic.oup.com/mnras/article/158/4/383/2603087 by guest on 26 January 2026

© Royal Astronomical Society • Provided by the NASA Astrophysics Data System

1972MNRAS.158..383D

Dinger, A. S., 1970. *Astrophys. Space Sci.*, **6,** 118.
Dinger, A. S., 1971. Unpublished Ph.D. thesis, Northwestern University.
Divine, N., 1965. *Astrophys. J.*, **142,** 824.
L'Ecuyer, J., 1966. *Astrophys. J.*, **146,** 845.
Fowler, W. A., Caughlan, G. R. & Zimmerman, B. A., 1967. *A. Rev. Astr. Astrophys.*, **5,** 525.
Hack, M., 1967. Hydrogen-poor Stars in *Modern Astrophysics*, ed. M. Hack, Gordon and Breach, New York.
Hayashi, C., Hoshi, R. & Sugimoto, D., 1962. *Prog. theor. Phys. Suppl., No.* **22.**
Hill, P. W., 1965. *Mon. Not. R. astr. Soc.*, **129,** 137.
Hubbard, W. B. & Lampe, M., 1969. *Astrophys. J.*, **156,** 795.
Hunger, K. & Klinglesmith, D. A., 1969. *Astrophys. J.*, **157,** 721.
Oke, J. B., 1961. *Astrophys. J.*, **133,** 166.
Osaki, Y., 1963. *Publ. astr. Soc. Japan*, **15,** 428.
Paczynski, B., 1969. *Acta Astr.*, **19,** 1.
Paczynski, B., 1970a. *Acta Astr.*, **20,** 47.
Pacyznski, B., 1970b. *Acta Astr.*, **20,** 195.
Paczynski, B., 1970c. *Acta Astr.*, **20,** 287.
Patterson, J. R., Winkler, H. & Zaidins, C. S., 1969. *Astrophys. J.*, **157,** 367.
Reeves, H., 1965. *Stellar Structure*, p. 165, eds L. H. Aller and D. B. McLaughlin, University of Chicago Press, Chicago.
Rose, W. K., 1966. *Astrophys. J.*, **144,** 1001.
Rose, W. K., 1969. *Astrophys. J.*, **155,** 491.
Tsuji, T., 1964a. *Ann. Tokyo Astr. Obs.*, **9,** 1.
Tsuji, T., 1964b. *Proc. Japan Acad.*, **40,** 99.
Van der Borght, R. & Meggitt, S., 1963. *Austr. J. Phys.*, **16,** 68.

Downloaded from https://academic.oup.com/mnras/article/158/4/383/2603087 by guest on 26 January 2026

© Royal Astronomical Society • Provided by the NASA Astrophysics Data System